Heliyon 7 (2021) e07767

Contents lists available at ScienceDirect

Heliyon

journal homepage: www.cell.com/heliyon

Research article

Sonoluminescence from ultra-high temperature and pressure cavitation produced by a narrow water jet

Toshihiko Yoshimura [a,*], Nobuaki Nishijima [a], Daiki Hashimoto [a], Masataka Ijiri [b]

[a] Department of Mechanical Engineering, Sanyo-Onoda City University, 1-1-1 Daigaku-dori, Sanyo-Onoda, Yamaguchi 756-0884, Japan
[b] Department of Mechanical Systems Engineering, Tokyo Metropolitan University, 1-1 Minami-Osawa, Hachioji, Tokyo 192-0397, Japan

ARTICLE INFO

Keywords:
Multifunction cavitation
High-pressure high-temperature cavitation
Narrow water jet nozzle
Multi-bubble sonoluminescence

ABSTRACT

This work developed a small-scale processing apparatus for ultra-high temperature and ultra-high-pressure cavitation (UTPC) incorporating a small diameter (0.1 mm) water jet nozzle. This instrumentation comprised a swirl flow nozzle (SFN) installed on the water jet nozzle so as to obtain UTPC from a multifunction cavitation (MFC) setup. Multi-bubble sonoluminescence (MBSL) assessments using two types of photon counting heads were employed to assess UTPC, MFC, ultrasonic cavitation (UC), water jet cavitation (WJC) and SFN-WJC. The SL intensity was found to increase in the order of SFN-WJC, WJC, UC, MFC to UTPC. Because UTPC produced the most intense emissions, this process evidently attained the highest processing temperature. Assuming a UC bubble temperature of 4000 K, the temperatures associated with UTPC, MFC and WJC were determined to be 5400–5900, 5300 and 3200–3300 K, respectively. The energy density of a single bubble during UTPC was calculated using the Rayleigh–Plesset and Planck equations for an initial bubble radius of 100 μm together with photon measurements from many bubbles and employing Planck's law. The highest SL intensity of UPTC is thought to exist due to the high energy density of UTPC. This research demonstrates that it is possible to increase the energy density of cavitation bubbles within a small reaction area.

1. Introduction

Sonoluminescence (SL) is a phenomenon whereby pulsating bubbles increase diffuse sound energy by up to 12 orders of magnitude (Barber and Putterman, 1991) to generate extremely short flashes of ultraviolet light (Putterman 1995; Putterman and Weninger 2000). There are two types of SL: single-bubble SL (SBSL) (Brenner et al. 2002) and multi-bubble SL (MBSL) (Sadighi-Bonabi et al., 2010; Didenko et al. 2000). As a result of adiabatic heating in water, the temperature inside a bubble can rise to 2300–5100 K during MBSL (William et al., 1999) and 5000–50,000 K in the case of SBSL (Barber et al., 1997; Brenner et al. 2002). Previously published MBSL spectra (Didenko and Pugach 1994; Matula et al., 1995) demonstrate that light emissions from excited molecules are not quenched during MBSL (SBSL: temperature 5000–10,000 K, pressure 10^9–10^{10} Pa, plasma light emission; MBSL: 300–5000 K, pressure 10^7–10^8 Pa, molecular light emission). This is because the pressure and temperature inside bubbles generated during MBSL are much lower than those during SBSL. Thus, the primary difference between SBSL and MBSL is the pressure and temperature achieved inside the bubbles. This suggests that, even in a cavitation bubble field, some of the bubble collapses will be SBSL-like such that molecular emissions will be highly quenched. Indeed, Giri and Arakeri (1998) reported that the MBSL and SBSL spectra will be similar in the case that the acoustic amplitude is sufficiently high.

The bubble temperature can be modified by both the buffer environment and the gas composition inside the bubble (Borissenok 2008; Moshaii et al., 2008). The spectrum of the emitted light tends to peak in the ultraviolet but is greatly affected by the gases dissolved in the liquid. As an example, traces of noble gases or other impurities can dramatically change the light emission intensity. However, this intensity is also affected by small variations in other operating parameters, including the forcing pressure, dissolved gas concentration and liquid temperature. The dynamics of SBSL strongly depend on the concentration of inert gases within the bubbles. In particular, the partial pressure of argon (or other gases) will determine the bubble stability. Argon rectification can occur in SBSL but not in MBSL because it requires bubble stability over many oscillation cycles. Our own group has also observed increased light intensity using a photon counting head during multifunction cavitation (MFC) in conjunction with argon bubbling in large-scale equipment (Yoshimura et al., 2020). In addition, the MBSL spectra of water in the

* Corresponding author.
E-mail address: yoshimura-t@rs.socu.ac.jp (T. Yoshimura).

https://doi.org/10.1016/j.heliyon.2021.e07767
Received 15 May 2021; Received in revised form 17 June 2021; Accepted 10 August 2021

presence of xenon have been shown to resemble the SBSL spectra (Hiller et al. 1998). These experimental spectra have been compared with both the blackbody spectrum of a body with an internal temperature of 20,000 K (Vazquez et al., 2002) and the spectrum of bremsstrahlung radiation given off by a plasma at 100,000 K (Wu and Roberts 1994). However, recent estimates of the true temperature are lower, falling between 6000 and 20,000 K (Brenner et al. 2002).

The results described above suggest that gas temperatures inside the bubbles are high, but there is still no universal agreement regarding the photon production mechanism. At these temperatures, the possible light production mechanisms include blackbody radiation, bremsstrahlung radiation and ion–electron recombination. All are thought to make a contribution to the spectrum, but the dominant process is believed to be recombination. The intense implosion of gas or vapor bubbles induced by acoustic cavitation can lead to ultra-strong compressions, high temperatures and light flashes due to SL.

Recently, we developed a system for ultra-high temperature and ultra-high-pressure cavitation (UTPC) processing. Although UTPC can be used in various industrial and research fields, it is particularly effective for micro-forging as a means of increasing the strength and functionality of various materials (Yoshimura et al., 2018b, 2019). Micro-forging forms a hardened layer on the outermost surface of a metal together with a very tough layer directly underneath this hardened layer. Conventional surface treatment technology only produces a hardened surface layer and cracks are likely to occur immediately below the surface when the material is exposed to external forces such as a thermal shock. Therefore, because UTPC also forms an underlying region with high toughness, it is expected that the occurrence of cracks directly under the surface hardened layer can be prevented (Ijiri and Yoshimura 2018). Previous research results have shown that micro-forging techniques (Ijiri et al. 2018, 2019) such as particle peening (Kikuchi et al. 2010), water jet peening, laser peening, nitridization and carburizing produce exceptional material properties that are not obtained with conventional surface treatments. Water jet nozzles with diameters from 0.7 to 2.0 mm have been used in large-scale processing equipment for water jet peening, MFC and micro-forging by UTPC to produce surface modification (Yoshimura et al., 2019, International PCT published patent WO2016136656A1, US registered patent, Inventor: Toshihiko Yoshimura, Assignee: Sanyo-Onoda City Public University, US Patent No. 10,590,966 B2, Date of Patent: Mar. 17, 2020).

Even so, the processing of fine powders, such as titanium oxide, at the nano-level by MFC (Yoshimura et al., 2016b; Yoshimura et al., 2018; International PCT published patent WO2016136656A1, US registered patent, Inventor: Toshihiko Yoshimura, Assignee: Sanyo-Onoda City Public University, US Patent No. 10,590,966 B2, Date of Patent: Mar. 17, 2020) or UTPC using conventional equipment in conjunction with a high flow rate requires a prolonged time period to collect and separate the water and powder after the treatment. As well, high-purity processing using pure water is difficult. When modifying the molecular structure (Sivalingam et al. 2004) of a substance using conventional ultrasonic cavitation (UC), it is likely that raising the temperature (that is, increasing the temperature inside the bubbles) will promote various chemical reactions. In view of the above requirements, one of the objectives of the present research was to develop compact UTPC equipment that enables tabletop reaction processing at a constant flow rate with a narrow nozzle.

In this study, we developed smaller-scale MFC and UTPC equipment with a narrow water jet nozzle having a diameter of 0.1 mm. Furthermore, the light emission intensities during MFC and UTPC were quantified using a photon counting head and the temperatures inside the multi-bubble were estimated from these data. The energy density of single bubbles during the UTPC process were calculated employing the Rayleigh-Plesset (Rayleigh, 1917; Plesset, 1949) and Planck equations and compared with the energy densities obtained from photon measurements of multiple bubbles and Planck's law. Finally, we assessed the feasibility of increasing the energy density of cavitation bubbles within a smaller reaction region.

2. Development of small-scale UTPC processing equipment

Figure 1 is a schematic diagram of the small-scale UTPC processing equipment developed in this work. The basic components of this apparatus are the same as those in the larger scale UTPC equipment previously used to impart high surface functionality, apply compressive residual stress, improve corrosion resistance and oxidation resistance, and induce peening aging. Processing systems based on high-pressure water jets have been used for decades in applications such as mining, industrial machining, cleaning and demolition (Summers 1995). Over this time span, the specific technique referred to as water jet cavitation (WJC) was developed (Kling 1970; Summers et al., 1987). The WJP method employs the phenomenon of cavitation collapse that takes place at the surface of a material subjected to a water jet at a pressure of at least 1000 MPa.

When the bubbles formed during the WJC process are irradiated with ultrasonic waves from the lateral direction, MFC occurs. In the case of UC processing, bubble nuclei with radius values of several micrometers originally present in the water expand isothermally and shrink adiabatically. In the same manner, during MFC, water jet bubbles with a radius of about 100 μm expand isothermally and shrink adiabatically, which leads to high-temperature and high-pressure cavitation. Furthermore, if a swirl nozzle is installed in the water jet nozzle, the nozzle outlet will decrease the static pressure while increasing the dynamic pressure, while the surrounding water flows into the swirl nozzle to generate a swirling flow. This lower pressure around the pressure water jet stream decreases the cavitation number, Ca, which increases the number of WJC bubbles as well as the size of the WJC. Because the initially large WJC bubbles increase in size when subjected to ultrasonic irradiation, the ratio of the isothermal expansion radius to the adiabatic compression radius increases such that numerous UTPC bubbles are generated.

Experimental and analytical studies have assessed both the non-steady state movement during WJC and the WJC bubble cloud distribution (Peng and Shimizu, 2013; Peng et al., 2018). The bubble cloud oscillation is significantly affected by the void fraction (that is, the volume fraction of bubbles). Specifically, a larger void fraction will reduce the cloud oscillation frequency to a greater extent than that of a single bubble and also cause the oscillation to decay much more slowly (Peng et al., 2015). In addition, UTPC increases both the quantity and size of WJC bubbles, and these effects are likely to raise the bubble cloud oscillation frequency while lowering the void ratio.

In the case of large UTPC equipment for surface modification, the pump discharge pressure is 35 MPa (this being the nominal maximum value), the flow rate is 7 L/min (the measured value), the diameter of the liquid jet nozzle is 0.8 mm (the measured value), the ultrasonic frequency is 28 kHz, the ultrasonic output power is 800 W, the reactor size is 45 × 41 × 60 cm (111 L) and a swirl flow nozzle is incorporated. In contrast, the reduced-size UTPC apparatus has a pump discharge pressure of 40 MPa (nominal maximum value), flow rate of 200 L/min (nominal maximum value), liquid jet nozzle diameter of 0.1 mm (target value), ultrasonic frequency of 28 kHz, ultrasonic output power of 40 W and reactor size of 25 × 16 × 20 cm (8 L). The ultrasonic transducer oscillation surface has a square geometry with each side having a length of 10 cm.

In comparison with a standard high-pressure pump, the small pump used in the present work had a higher pressure but an extremely low flow rate of 150 mL/min. As a result, the size of the reaction tank was reduced and an equipment configuration for chemical reaction experiments that could fit on a tabletop became possible. Based on the nozzle cross-sectional area and the flow rate per unit time, the flow velocity at the standard nozzle outlet was 230 m/s while that at the small nozzle was 420 m/s. An ultrasonic frequency of 28 kHz was selected as the resonance frequency because bubble expansion and contraction were maximized at this frequency for both sizes of equipment setups. The resonance

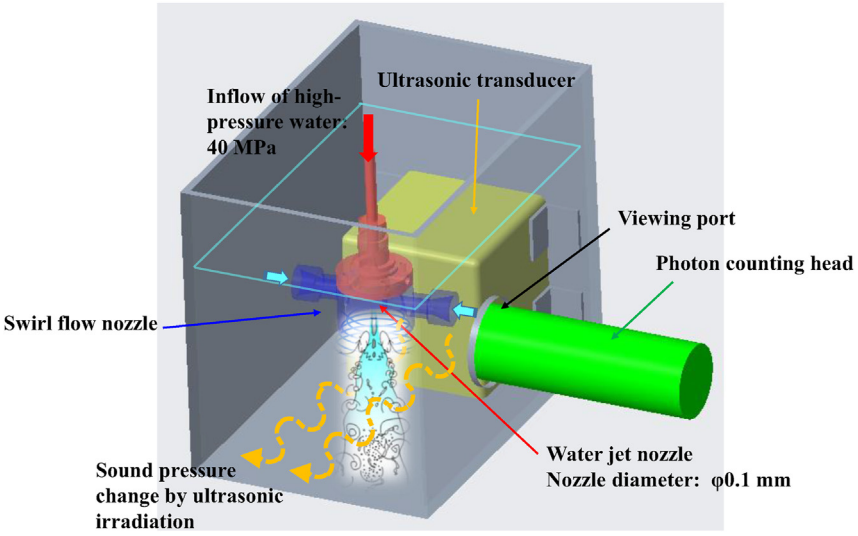

Figure 1. Schematic diagram of small-scale equipment for processing by ultra-high temperature and pressure cavitation.

frequency at which bubbles will vibrate most violently can be obtained using the Minnaert formula (Minnaert, 1933; Yoshimura et al., 2016a). For water jet cavitation with bubbles having a radius of 100 μm, the resonance frequency is 33 kHz, while the value for larger bubbles is 28 kHz. Water jet cavitation bubbles used for the surface modification of materials are known to have a radius of 100 μm, but there are no data available concerning the bubble sizes produced by narrow nozzles. The radius of the cavitation bubbles is thought to decrease with a smaller nozzle radius, and so the number and size of the bubbles were increased by halving the size of the swirl nozzle previously used in the large-scale equipment. Various swirl nozzles were mounted on the WJC nozzle in the large-scale processing equipment, and a swirl nozzle capable of achieving high temperature and high functionality bubbles was investigated. As a result, it became clear that, due to the two inflow holes in the equipment, it was beneficial to taper the inside of the swirl flow nozzle (Yoshimura et al., 2018b, 2019). The ultrasonic transducer was manufactured by Honda Electronics Co., Ltd. (HEC-45282, 50 W) and had an actual output power of 40 W.

The H9319 series photon counting heads (Hamamatsu Photonics K.K.) used in this work were designed to perform photon counting and provide results with a simple PC connection. The H9319 series included a 25 mm diameter head-on photomultiplier tube, a photon counting circuit, a high-voltage power supply circuit, a counter and a microprocessor. A single photon striking the photocathode was converted into a single electron and the collision of this electron with the first dynode generated an avalanche process involving multiple dynodes. Two versions of the H9319 photon detector were used: the H9319-01 and H9319-02. The main difference between these two devices was that the latter had higher sensitivity at higher wavelengths. Specific details are provided in the Results section.

Figure 2 shows the manufacturing procedure for the narrow nozzle. Because the size and shape of the nozzle hole affected the cavitation characteristics, a large number of holes each with a diameter of approximately 0.1 mm were produced in a flat, 1.8 mm thick plate using an electric discharge device. The size and roundness of each hole was subsequently assessed using an optical microscope and two holes with a small difference in diameter between their front and back openings were selected. The results of these optical microscopy observations are shown in Figure 3. Disks containing each hole were cut from the plate, and the upstream and downstream parts were combined and welded together, as shown in Figure 2, to complete the narrow nozzle.

It should be noted that we also attempted to form the holes using a precision drilling device but were unable to produce a hole with a diameter of 0.1 mm in a plate with a thickness of 1 mm or more. A 1 mm

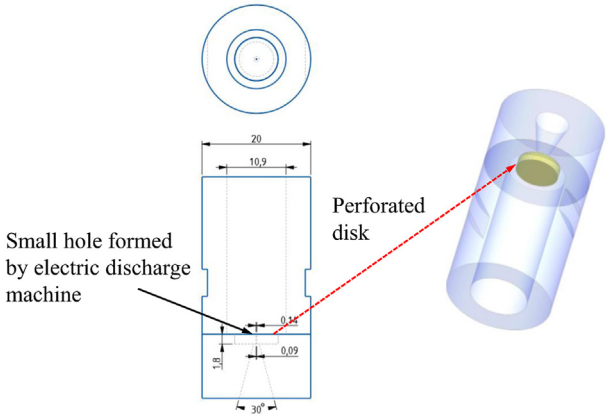

Figure 2. Manufacturing procedure for narrow nozzle.

thick plate could not be used because it was unable to withstand the high pressure associated with this process. The high-pressure pump had a maximum discharge pressure of 40 MPa and a maximum flow rate of 200 mL/min. To generate an effective cavitation jet, a hole having a suitable diameter in the range from 0.1 to 0.2 mm had to be formed. Drilling with a laser or electron beam was also considered, but the cost of these methods was excessive. During operation of the electric discharge apparatus (Mitsubishi Electric Corp.), a discharge was generated between the test piece and an electrode with a diameter of 0.1 mm, and the machining was performed by changing the distance between the electrode and the test piece. This was found to be the most suitable technique for making the type of hole required for the pressure and flow rate associated with the high-pressure pump used in this study.

We also reduced the size of the swirl flow nozzle used for UTPC. A high-pressure water jet nozzle fabricated using the two disks with holes (Figure 4) gave a flow rate and pressure of 195 cm^3/min and 20 MPa, respectively, with the 0.17 mm nozzle and 155 cm^3/min and 40 MPa with the 0.09 mm nozzle. The latter was chosen for use in the experiments because this smaller nozzle had the advantage of generating a higher pressure.

3. Experimental method

Figure 5 provides a photographic image of the small-scale equipment used for UTPC processing and for measuring the light intensity during

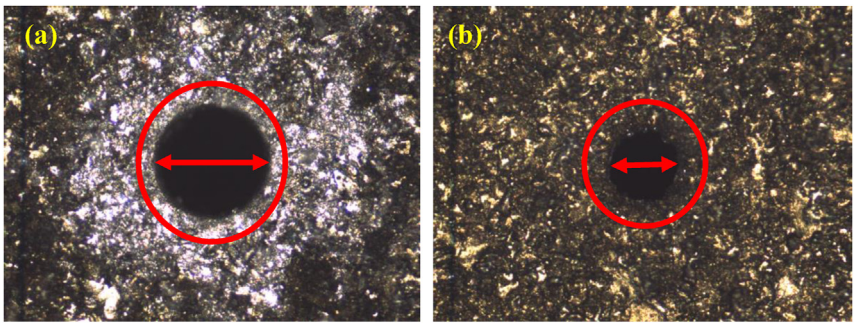

Figure 3. Optical microscopic observation of holes for the narrow nozzle: (a) Hole with 0.17-mm diameter and (b) Hole with 0.094-mm diameter.

Figure 4. Narrow water jet nozzles and swirl flow nozzle.

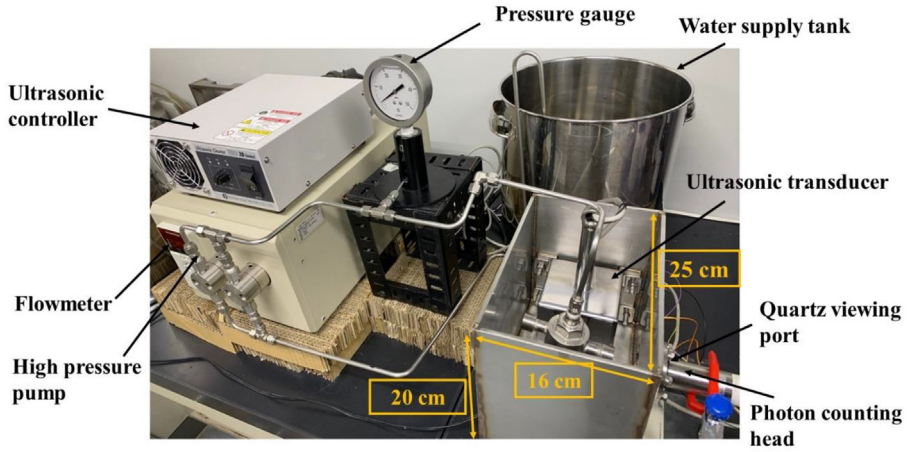

Figure 5. Small-scale equipment for UTPC processing and measurement of light intensity.

cavitation in the present work. As noted, all the equipment used in these experiments, such as the high-pressure pump (L. TEX Corp., LTEX8731E) and the ultrasonic output device, were reduced in size, which made it possible to place them on a table and also reduced the noise output during the process. Photon counts were obtained during processing using the UC, WJC, MFC, WJC with swirl flow nozzle (that is, SFN-WJC) and UTPC (SFN-MFC) techniques. During these trials, the flow rate was 155 cm^3/min, the pump pressure was 40 MPa, the sampling interval of the photon counting head was 1 s and the total measurement time was 600 s. The light emission intensity during cavitation was measured through a quartz viewing port using two types of photon counting heads.

The quartz viewport was attached to a ConFlat flange that was used as an ultra-high vacuum component and was completely waterproof. Quartz glass transmits ultraviolet to visible wavelengths to a greater extent than other types of glass and so was most suitable for measuring the emission intensity of the cavitation bubbles. Either tap water from a stainless-steel water supply tank, pure water or ultrapure water supplied from a high-pressure pump was employed, depending on the purpose. The flow rate of the water jet was ascertained using a flow meter installed in the high-pressure pump, while the water jet pressure was measured by a pressure gauge installed on the water jet nozzle side. During each trial, the entire apparatus was covered with a dark curtain to shield it from ambient light. Even so, hundreds of stray photons were detected every second in the absence of processing. However, because the UTPC system generated hundreds of thousands of photons per second, and even the SFN-WJC system (which had the lowest emission intensity) produced thousands of photons, the effect of incident light from the surroundings was negligible. Despite this, the amount of incident light from the

surroundings was monitored for each measurement condition and the average number of photons per second was subtracted from the measurement value for each cavitation generation condition to obtain the final measured value.

4. Results and discussion

The light intensity data obtained with the H9319-01 photon counting head for various cavitation methods are shown in Figure 6. The values for the WJC and SFN-WJC processes were very low and generally did not fluctuate over time. The light intensity produced during UC was also less than that of the MFC and UTPC trials because the larger bubbles produced by WJC were irradiated by ultrasonication to a greater extent. Consequently, these bubbles expanded greatly and shrank extremely rapidly based on variations in sound pressure, which produced temperature increases inside the bubbles. The UTPC and MFC emission intensities fluctuated greatly but were generally high. The SFN-WJC showed the lowest light intensity because the water jet bubbles generated by the swirl flow nozzle had low internal pressures during shrinkage in the swirl flow nozzle, even if the bubbles were large.

Figure 7 shows the results obtained with the H9319-02 counting head. As with the H9319-01 head, the light intensity increased in the order of WJC, MFC to UTPC. In contrast to the H9319-01 head, the light intensity of the UTPC process was greater than that measured during the MFC process, indicating that the bubble temperature was increased by the swirl flow nozzle. These results also indicate that the UPTC method exhibited especially high emissions in the high wavelength region of the spectrum. The light intensity increased in the order of SFN-WJC, WJC, UC, MFC to UTPC. These results suggest that the UTPC method generated the highest temperature, in accordance with the results of the previous high-temperature processing of various materials by UTPC with a 0.8 mm nozzle (Yoshimura et al., 2020). Figures 6 and 7 present the average photon counts. Note that a measurement uncertainty of approximately 5%–6% can be assumed as a result of the effects of uncertainties in the WJ nozzle, counting head and SFN nozzle installation positions.

It is known from previous experiments with SBSL (Hammer and Frommhold 2000) that the resulting spectra are similar to a Planck black body radiation spectrum (Planck et al., 1914). A blackbody completely absorbs all incident light, such that the light emitted from the blackbody is determined only by the temperature. Planck introduced a discrete photon energy of $h\nu$ in the energy equation for blackbody radiation and obtained the equation:

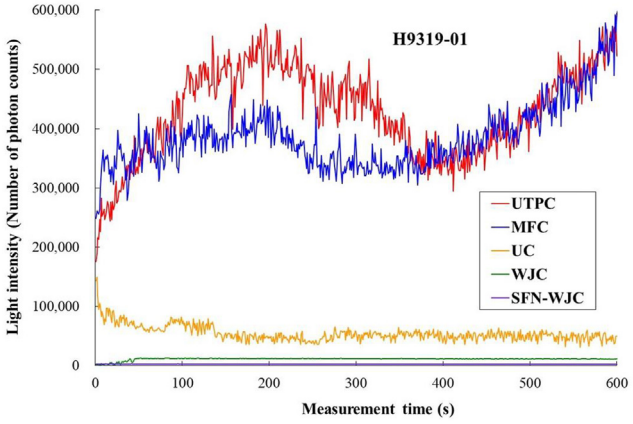

Figure 6. Measurement results of light intensity for various cavitation methods (H9319-01 counting head). (Average value of photon counts: UTPC 429,226, MFC 384,896, UC 54,440, WJC 11,259, SFN-WJC 2,700).

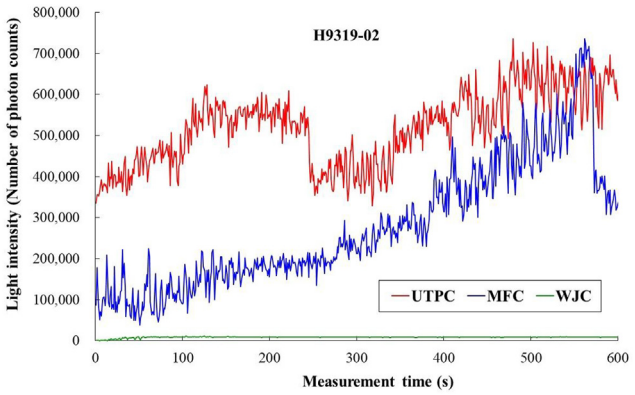

Figure 7. Measurement results of light intensity for various cavitation methods (H9319-02 counting head). (Average value of photon counts: UTPC 520,230, MFC 276,442, WJC 8,591).

$$I^{pl} = \frac{2hc^2}{\lambda^5} \frac{1}{\exp(\frac{hc}{\lambda k_B T}) - 1} \quad (1)$$

where I^{pl} is the energy density ($J{\cdot}s^{-1}{\cdot}m^{-2}{\cdot}sr^{-1}{\cdot}m^{-1}$), h is Planck's constant (6.626×10^{-34}J·s), ν is the frequency of light (Hz), c is the speed of light in the medium (material or vacuum, m/s), λ is the wavelength (m), k_B is the Boltzmann constant (1.38×10^{-23}J/K), and T is temperature (K). A feature of Eq. (1) is that the maximum value shifts toward the ultraviolet region as the temperature rises.

From the equation $c = \lambda\nu$, it is apparent that energy emitted at shorter wavelengths increases more rapidly with temperature than does energy emitted at longer wavelengths. This law may also be expressed in other terms, such as with regard to the number of photons emitted at a certain wavelength or the energy density in a given volume of radiation.

The energy density calculated by Planck's black body radiation method was corrected by the counting sensitivity. Assuming that the UC bubble temperature was 4000 K, the temperature was estimated by selecting an energy density curve that was consistent with the light intensity ratios between the measured values for the various cavitation methods. Using the H9319-01 counting head, the temperature obtained during UTPC processing was determined to be 5400 K, while the values for MFC, WJC and SFN-WJC were 5300, 3300 and 2900 K, respectively. For the H0310-02 head, the UTPC, MFC, WJC and SFN-WJC temperatures were 5900, 5300, 3200 and 2700 K.

Titanium oxide powder and platinum powder, acting as co-catalysts, were processed using the newly developed UTPC equipment with a water jet nozzle having a 0.1 mm diameter (Yoshimura et al., 2021). The water was subsequently evaporated to collect the processed powder, which was then introduced into a vacuum and irradiated with visible light from a light emitting diode (LED). Hydrogen generated by the decomposition of water contained in the powder was quantified using a quadrupole mass spectrometer (Yoshimura, Tanaka, and Yoshinaga 2018a; Yoshimura, Tanaka, and Ijiri 2018b). The results showed that the UTPC process generated the most hydrogen, in agreement with the light emission intensity data.

Increasing the energy density of cavitation bubbles in a smaller reaction region is very important in terms of improving the functionality and reaction efficiency of various materials. In the case of ultrasonic cavitation systems used in cleaning equipment, bubbles that are originally floating in the water (that is, bubble nuclei) are repeatedly isothermally expanded and adiabatically compressed due to changes in the sound pressure of ultrasonic waves, and the temperature inside the bubbles rises. As noted, as the initial bubbles increase in size, the temperature inside the bubbles increases exponentially during contraction. Figure 8 shows the fluctuations in energy density at a wavelength of $\lambda =$ 800 nm (determined by Planck's law as shown in Eq. (1)) when UC bubbles with a radius of 4 μm and WJC bubbles with a radius of 100 μm

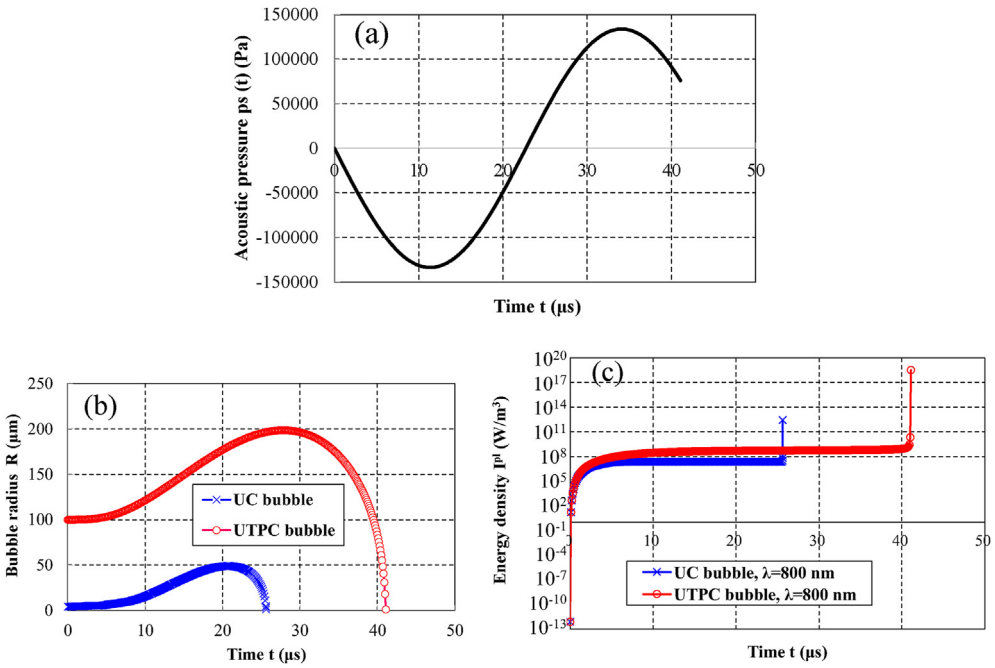

Figure 8. Energy density of photons from bubbles at 800 nm and internal pressures and temperatures of bubbles during UC and UTPC (UC: 4 μm ⇒ 1 μm, UTPC: 100 μm ⇒ 1 μm): (a) Acoustic pressure (b) Bubble radius and (c) Energy density of photons from bubble.

are subjected to a sound pressure of 1.3 Pa and shrink to 1 μm. In the case of the UC bubbles, the energy density is 2.67×10^{12} at a bubble radius of 1 μm, whereas the value for the MFC bubbles is 3.27×10^{18} at the same radius, representing an increase of six orders of magnitude. Prior work has estimated the temperatures that are achieved during bubble contraction using the Rayleigh–Plesset and Keller–Miksis equations (Keller and Miksis 1980) for various initial bubble sizes. In the present work based on SBSL, the pressures and temperatures during the contraction of 4 μm (UC) and 100 μm (UTPC) bubbles were calculated using the Rayleigh-Plesset equation. The resulting temperatures were then employed in conjunction with Planck's equation to determine energy densities based on wavelength.

The expansion and contraction of bubbles can be modeled via the Rayleigh-Plesset equation:

$$R\ddot{R}+\frac{3\dot{R}^2}{2}=\frac{1}{\rho}\left(p_g+p_v-\frac{2\sigma}{R}-\frac{4\mu\dot{R}}{R}-p_0-p_s(t)\right) \quad (2)$$

where R is the radius of the bubble, p_g, p_0, p_v and $p_s(t)$ are the gas, static, vapor and sound pressure at time t, respectively, and σ is the surface tension. The rate of acceleration can then be calculated as:

$$\ddot{R}=-\frac{3\dot{R}^2}{2R}+\frac{1}{\rho R}\left(p_g+p_v-\frac{2\sigma}{R}-\frac{4\mu\dot{R}}{R}-p_0-p_s(t)\right) \quad (3)$$

When working with the MBSL data, energy density calculations were performed for different wavelengths and temperatures based on the Planck equation. Following this, the energy density values were corrected based on the sensitivity at each wavelength associated with Detectors 1 and 2 (Yoshimura et al., 2020). Lastly, the rates of increase in the average sensitivity-corrected energy density values were determined at specific temperatures with respect to 4000 °C of UC. The results indicated the temperatures for which the rates of increase relative to the UC energy density equaled the rates of increase in the quantity of photons received by the two detectors during WJC, MFC, SFN-WJC and SFN-MFC (UTPC) processing. These temperature values were subsequently used in conjunction with Planck's equation to find energy densities based on wavelength and temperature for specific experimental conditions. The results provide the first demonstration of the correlation between energy density and wavelength for the UC and MFC techniques during bubble contraction, as determined using solely the Rayleigh–Plesset equation.

Assuming that the law of similarity in fluid dynamics holds, the WJC bubbles will be smaller when using the 0.1 mm nozzle compared with the 0.8 mm nozzle. It is thought that the sizes of WJC bubbles generated from the 0.1 mm nozzle are between the bubble radius of 100 μm generated from the 0.8 mm nozzle and the bubble nuclei radius of several micrometers. The radius of the WJC bubbles used for peening, generated with a nozzle diameter of 0.8 mm, is approximately 100 μm but this value is increased when a swirl nozzle (intended for UTPC) is installed to the WJ nozzle. Similarly, if a swirl nozzle is attached to a 0.1 mm nozzle, the bubble radius will increase to within the range of several to 100 μm.

It has been experimentally determined that the light emission intensity during MBSL is lower than that associated with SBSL due to the interactions between bubbles. Figure 9 shows the relationships between the emission wavelength and energy density for both MBSL and SBSL under various conditions. If the UTPC bubbles are considered as a single bubble, the multi-bubble UTPC energy density in Figure 9 becomes higher. Therefore, the energy density of a single bubble in UTPC is between the energy density graph obtained from the Rayleigh–Plesset equation and Planck's equation for a single bubble with an initial radius of 100 μm and that obtained from the energy density graph generated based on photon measurements from multiple bubbles and Planck's law. It should be noted that the energy density for multiple bubbles obtained from the photon measurements during UTPC with a swirl nozzle attached to the 0.1 mm WJ nozzle and Planck's equation was higher than that for a single bubble as determined using the Rayleigh–Plesset and Planck's equations for 4 μm UC. This suggests that the increase in energy density due to the increase in bubble size is greater than the decrease in energy density due to the interactions of multiple bubbles. From the above results, it can be concluded that the newly developed smaller UTPC device provided more highly concentrated bubble energy. This study thus demonstrates that it is possible to increase the energy density of cavitation bubbles within a smaller reaction region, which is very important to improving the functionality and reaction efficiency of various materials.

It should be noted that, because ultrasonic waves were applied to the water jet cavitation system from one direction in the present work, the energy concentration of the bubbles was not maximized. If the energy-

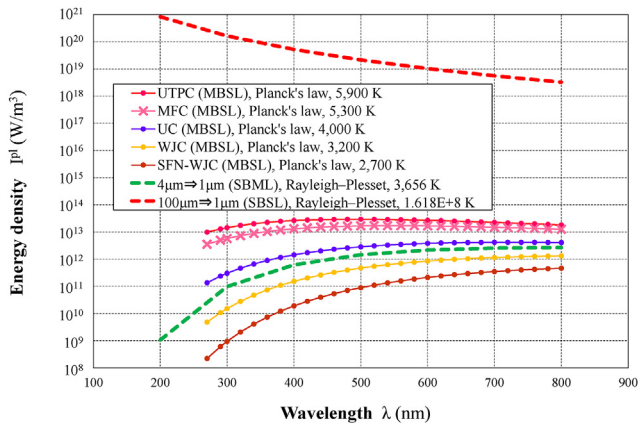

Figure 9. Energy density comparison of single-bubble sonoluminescence (SBSL) calculated by Rayleigh–Plesset equation and multi-bubble sonoluminescence (MBSL) calculated by Planck's law at the estimated temperature based on experimental value (H9319-02 counting head).

concentrated nozzle were to be irradiated with ultrasonic waves from the circumferential direction, the bubble temperature and pressure would be greatly increased and the degree of material processing would be significantly improved. Therefore, if an energy-concentrated nozzle can be developed for this smaller UTPC device, the energy density of the bubbles in Figure 9 would be expected to increase further.

5. Conclusions

This work developed small-scale processing equipment to allow UTPC with a narrow water jet nozzle (diameter of 0.1 mm). This apparatus was used to investigate the MBSL associated with the UTPC, MFC, UC, WJC and SFN-WJC processing methods using two types of photon counting heads. The following conclusions can be made.

(1) The light intensity increases in the order of SFN-WJC, WJC, UC, MFC, to UTPC. These results suggest that the UTPC method generates the highest temperatures, in accordance with the results of high-temperature materials processing using this technique.
(2) Assuming a UC bubble temperature of 4000 K, the UTPC, MFC and WJC bubble temperatures are 5400–5900, 5300 and 3200–3300 K, respectively.
(3) The energy density of a single bubble during UTPC processing is between the values obtained from the Rayleigh–Plesset equation and the energy density of one bubble during UTPC obtained using Planck's law at the temperature estimated from the experimental results.
(4) It is possible to increase the energy density of cavitation bubbles within a smaller reaction area.

Declarations

Author contribution statement

Toshihiko Yoshimura: Conceived and designed the experiments; Analyzed and interpreted the data; Wrote the paper.

Nobuaki Nishijima, Daiki Hashimoto & Masataka Ijiri: Performed the experiments; Analyzed and interpreted the data.

Funding statement

This work was supported by the Japan Society for the Promotion of Science, KAKENHI Grants 16K06029 and 19K04110 (Grant-in-Aid for Scientific Research C) and by the Light Metal Educational Foundation.

Data availability statement

Data included in article/supp. material/referenced in article.

Declaration of interests statement

The authors declare no conflict of interest.

Additional information

No additional information is available for this paper.

References

Barber, B.P., Putterman, S., 1991. Observation of synchronous picosecond sonoluminescence. Nature (London) 352, 318–320.
Barber, B.P., Hillerb, R.A., Löfstedt, R., Putterman, S.J., Weninger, K.R., 1997. Defining the unknowns of sonoluminescence. Phys. Rep. 281, 65–143.
Borissenok, V.A., 2008. Sonoluminescence: two sources of light. Phys. Lett. 372, 3496–3500.
Brenner, M.P., Hilgenfeldt, S., Lohse, D., 2002. Single-bubble sonoluminescence. Rev. Mod. Phys. 74, 425–484.
Didenko, Y.T., Pugach, S.P., 1994. Spectra of water sonoluminescence. J. Phys. Chem. 98, 9742–9749.
Didenko, Y.T., McNamara, W.B., Suslick, K.S., 2000. Effect of noble gases on sonoluminescence temperatures during multibubble cavitation. Phys. Rev. Lett. 84 (4), 777–780.
Giri, A., Arakeri, V.H., 1998. Measured pulse width of sonoluminescence flashes in the form of resonance radiation. Phys. Rev. E 58, R2713–R2716.
Hammer, D., Frommhold, L., 2000. Spectra of sonoluminescent rare-gas bubbles. Phys. Rev. Lett. 85, 1326–1329.
Hiller, R.A., Putterman, S.J., Weninger, K.R., 1998. Time-resolved spectra of sonoluminescence. Phys. Rev. Lett. 80 (8), 1090–1093.
Ijiri, M., Yoshimura, T., 2018. Evolution of surface to interior microstructure of SCM435 steel after ultra-high-temperature and ultra-high-pressure cavitation processing. J. Mater. Process. Technol. 251, 160–167.
Ijiri, M., Okada, N., Kanetou, S., Yamamoto, M., Nakagawa, D., Tanaka, K., Yoshimura, T., 2018. Thermal stress relaxation and high-temperature corrosion of Cr-Mo steel processed using multifunction cavitation. Materials 11, 2291.
Ijiri, M., Shimonishi, D., Tani, S., Okada, N., Yamamoto, M., Nakagawa, D., Tanaka, K., Yoshimura, T., 2019. Improvement of corrosion resistance of magnesium alloy by high-temperature high-pressure cavitation treatment. Int. J. Lightweight Mater. Manufact. 2, 255–260.
Keller, J.B., Miksis, M., 1980. Bubble oscillations of large amplitude. J. Acoust. Soc. Am. 68 (2), 628–633.
Kikuchi, S., Nakahara, Y., Komotori, J., 2010. Fatigue properties of gas nitrided austenitic stainless steel pre-treated with fine particle peening. Int. J. Fatig. 32, 403–410.
Kling, C.L., 1970. A High Speed Photographic Study of Cavitation Bubble Collapse. University Michigan. Report No. 03371-2-T, 08466-7-T.
Matula, T.J., Roy, R.A., Mourad, P.D., McNamara III, W.B., Suslick, K.S., 1995. Comparison of multibubble and single-bubble sonoluminescence spectra. Phys. Rev. Lett. 75, 2602–2605.
Minnaert, M., 1933. On musical air-bubbles and the sound of running water. Philos. Mag. 16 (104), 235–248.
Moshaii, A., Rezaei-Nasirabad, R., Imani, K., Silatani, M., Sadighi-Bonabi, R., 2008. Role of thermal conduction in single-bubble cavitation. Phys. Lett. A 372, 1283–1287.
Plesset, M.S., 1949. The dynamics of cavitation bubbles. J. Appl. Mech. 16, 277–282.
Peng, G., Shimizu, S., 2013. Progress in numerical simulation of cavitating water jets. J. Hydrodyn. 25, 502–509.
Peng, G., Oguma, Y., Shimizu, S., 2018. Numerical simulation of unsteady cavitating jet by a compressible bubbly mixture flow method. IOP Conf. Ser. Earth Environ. Sci. 163, 012037.
Peng, G., Tryggvason, G., Shimizu, S., 2015. Two-dimensional direct numerical simulation of bubble cloud cavitation by front-tracking method. IOP Conf. Ser. Mater. Sci. Eng. 72, 012001.
Planck, M., 1914. The Theory of Heat Radiation. Masius, M. (transl.), second ed. P. Blakiston's Son & Co. OL 7154661M.
Putterman, S., 1995. Sonoluminescence: sound into light. Sci. Am. 272 (2), 46–51.
Putterman, S., Weninger, K., 2000. Sonoluminescence: how bubbles turn sound into light. Annu. Rev. Fluid Mech. 32, 445–476.
Rayleigh, L., 1917. On the pressure developed in a liquid during the collapse of a spherical cavity. Philos. Mag. 34 (200), 94–98.
Sadighi-Bonabi, R., Rezaee, N., Ebrahimi, H., Mirheydari, M., 2010. Interaction of two oscillating sonoluminescence bubbles in sulfuric acid. Phys. Rev. E 82, 016316-1–016316-7.
Sivalingam, G., Agarwal, N., Madras, G., 2004. Distributed midpoint chain scission in ultrasonic degradation of polymers. AIChE J. 50 (9), 2258–2265.
Summers, D.A., 1995. Waterjetting Technology. E. & F. N. Spon, London.
Summers, D.A., Tyler, L.J., Blaine, J., Fossey, R.D., 1987. Considerations in the design of a waterjet device for reclamation of missile casings. In: Proc. of the Fourth U.S. Water Jet Conference. The University of California, Berkeley CA, pp. 82–89.

Vazquez, G., Camara, C., Putterman, S.J., Weninger, K., 2002. Blackbody spectra for sonoluminescing hydrogen bubbles. Phys. Rev. Lett. 88, 197402-1–197402-4.
William, B., McNamara III, W.B., Didenko, Y.T., Suslick, K.S., 1999. Sonoluminescence temperatures during multi-bubble cavitation. Nature 401, 772–775.
Wu, C.C., Roberts, P.H., 1994. A model of sonoluminescence. Proc. R. Soc. A 445, 323–349.
Yoshimura, T., Tanaka, K., Yoshinaga, N., 2016a. Development of mechanical-electrochemical cavitation technology. J. Jet Flow Eng. 32 (1), 10–17.
Yoshimura, T., Tanaka, K., Yoshinaga, N., 2016b. Material processing by mechanical-electrochemical cavitation. Proc. of 23nd International Conference Water Jetting 223–235.
Yoshimura, T., Tanaka, K., Yoshinaga, N., 2018a. Nano-level material processing by multifunction cavitation. Nanosci. Nanotechnol. - Asia 8 (1), 41–54.
Yoshimura, T., Tanaka, K., Ijiri, M., 2018b. Nanolevel surface processing of fine particles by waterjet cavitation and multifunction cavitation to improve the photocatalytic properties of titanium oxide. IntechOpen Cavitation. IntechOpen Limited, 5 Princes Gate Court, London, SW7 2QJ, UK.
Yoshimura, T., Ijiri, M., Shimonishi, D., Tanaka, K., 2019. Micro-forging and peening aging produced by ultra-high-temperature and pressure cavitation. Int. J. Adv. Technol. 10 (1), 227.
Yoshimura, T., Maeda, D., Ogi, T., Kato, F., Ijiri, M., 2020. Sonoluminescence from ultra-high-temperature and high pressure cavitation and its effect on surface modification of Cr-Mo steel. Global J. Technol. Optim. 11 (2).
Yoshimura, T., Shimonishi, D., Hashimoto, D., Nishijima, N., Ijiri, M., 2021. Effect of processing degree and nozzle diameter on multifunction cavitation. Surf. Eng. Appl. Electrochem. 57 (1), 106–116.